Current Carrying Capacity of Quasi-1D $ZrTe_3$ Van Der Waals Nanoribbons

A. Geremew, M. A. Bloodgood, E. Aytan, B. W. K. Woo, S. R. Corber, G. Liu, K. Bozhilov, T. T. Salguero, S. Rumyantsev, M. P. Rao, *Senior Member, IEEE*, and A. A. Balandin, *Fellow, IEEE*

***Abstract*— Quasi-1D van der Waals materials, such as transition metal trichalcogenides, have strong covalent bonds in one direction and weaker bonds in cross-plane directions. They can be prepared as crystalline nanowires or nanoribbons consisting of 1D atomic threads, i.e., chains. We have examined the current carrying capacity of $ZrTe_3$ nanoribbons using a set of structures fabricated by the shadow mask method. The bulk crystals were synthesized by the chemical vapor transport method and exfoliated onto Si/SiO_2 substrates. It was found that $ZrTe_3$ nanoribbons reveal an exceptionally high current density, on the order of ~100 MA/cm^2, at the peak of the stressing DC current. The low-frequency noise was of $1/f$ type near room temperature (f is the frequency). The noise amplitude scaled with the resistance, following the trend established for other low-dimensional materials. The high current density in $ZrTe_3$ can be attributed to the single-crystal nature of quasi-1D van der Waals materials.**

***Index Terms*— Van der Waals materials, quasi-1D Materials, nanowires; interconnects, current density, $ZrTe_3$.**

I. Introduction

AS AGGRESSIVE scaling in the complementary metal-oxide semiconductor (CMOS) technology continues, there is a growing need to examine new materials that can be used for nanometer-scale local interconnects or device channels [1], [2]. More than a decade ago, the industry moved from aluminum (Al) to copper (Cu) to lower resistance and improve reliability via reduced electromigration. Recently, it has been reported that the 10-nm logic technology node features local interconnects made of cobalt (Co), which enables a 10-fold reduction in electromigration [2]. At present, the current density sustained by Cu interconnects in state-of-the-art CMOS technology is between 2 MA/cm^2 to 3 MA/cm^2 [3], [4].

We recently proposed that quasi-one-dimensional (1D) van der Waals materials, such as transition metal trichalcogenides (TMTs) with formula MX_3 (where M = Nb, Ta, Ti, Zr, and other transition metals; X = S, Se, Te), have properties attractive for applications in nm-scale electronics. In a way similar to transition metal dichalcogenides (TMDs), which exfoliate into 2D layers [5], [6], TMTs exfoliate into quasi-1D atomic thread bundles [7]–[9]. We previously reported that metallic $TaSe_3$ nanowires have breakdown current density, at the peak of the stressing DC current, on the order of ~10 MA/cm^2 [7], [8]. In principle, such quasi-1D materials could be ultimately downscaled by exfoliation, or grown directly, into nanowires with a cross-section of ~1 nm × 1 nm, which corresponds to an individual atomic thread, *i.e.* chain.

Here we show that nanoribbons made of $ZrTe_3$, another member of the TMT family, reveal exceptionally high current density, on the order of ~100 MA/cm^2, at the peak of the stressing DC current (with a cross-section of ~27 nm × 450 nm). Our experimental data also indicate that the low-frequency noise (LFN), another important metric of the material's applicability in electronics, is relatively low, and scales down with the resistance, following the trend found for some other low-dimensional materials.

II. Material Synthesis and Characterization

The selection of $ZrTe_3$ was based on reports indicating that $ZrTe_3$ has better electrical conduction properties than other MX_3 materials [10]. For this study, $ZrTe_3$ crystals were synthesized by the chemical vapor transport (CVT) method [7], [8], [11], [12]. $ZrTe_3$ crystallizes in the monoclinic space group $P2_1/m$. It has strongly anisotropic electronic transport properties, and its bulk electrical resistivity is lower than that of $TaSe_3$ and several other MX_3 [12]–[15]. However, there are inconsistencies in the literature with respect to the reported electronic band structure of $ZrTe_3$, *i.e.* metallic *vs.* semiconducting, type of conduction, as well as in the transition temperatures to the charge density wave and superconducting

Manuscript received February 24, 2018; revised March 21, 2018; accepted March 23, 2018. Date of publication March 29, 2018; date of current version April 24, 2018. This work was supported in part by the Semiconductor Research Corporation under Contract 2018-NM-2796, in part by the National Science Foundation (NSF) under Award CMMI-1254999, and in part by NSF through the Emerging Frontiers of Research Initiative (EFRI) 2-DARE under Award EFRI-1433395. The review of this letter was arranged by Editor H. G. G. Xing. *(Corresponding author: Alexander A. Balandin.)*

A. Geremew, E. Aytan, G. Liu, S. Rumyantsev, and A. A. Balandin are with the Department of Electrical and Computer Engineering, University of California at Riverside, Riverside, CA 92521 USA (e-mail: balandin@ece.ucr.edu).

M. A. Bloodgood and T. T. Salguero are with the Department of Chemistry, The University of Georgia, Athens, GA 30602 USA.

B. W. K. Woo, S. R. Corber, and M. P. Rao are with the Department of Mechanical Engineering, University of California at Riverside, Riverside, CA 92521 USA.

K. Bozhilov is with the Materials Science and Engineering Program, University of California at Riverside, Riverside, CA 92521 USA.

Color versions of one or more of the figures in this letter are available online at http://ieeexplore.ieee.org.

Digital Object Identifier 10.1109/LED.2018.2820140

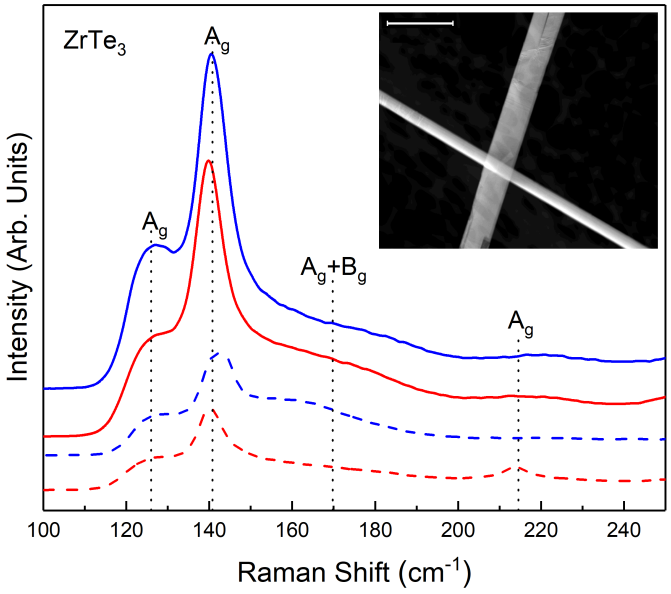

Fig. 1. Raman spectra of $ZrTe_3$ for CVT bulk (solid blue) and reference bulk (solid red). The data for exfoliated nanoribbons are shown by dashed lines of the corresponding colors. All spectra were recorded under 633 nm laser excitation and power below 1.5-mW on the surface, to avoid local heating. Inset shows TEM image of the CVT grown exfoliated $ZrTe_3$ crystal. The scale bar is 2 μm.

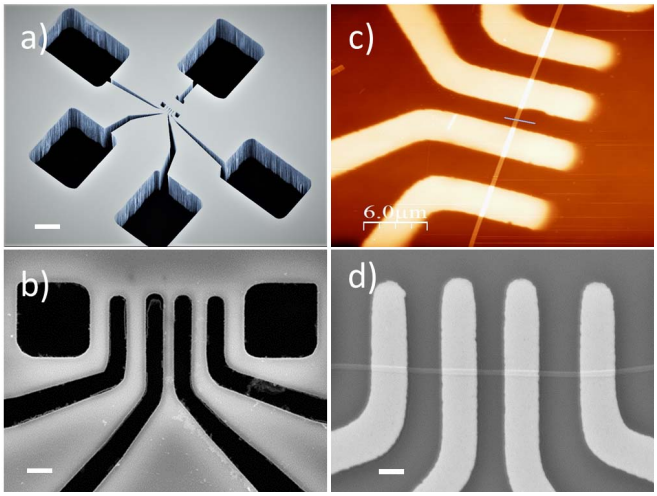

Fig. 2. (a) SEM image of a shadow mask with TLM stencil structure patterned on 500-μm thick Si/SiO_2 wafer. (b) Top-view SEM image of the pattern for Ti and Au evaporation to create the source and drain contacts. (c) AFM image of the quasi-1D $ZrTe_3$ nanoribbon device, fabricated using the shadow mask. AFM characterization was used to determine the nanowire width and thickness (~33-nm in the present case). (d) SEM image of another quasi-1D $ZrTe_3$ nanowire device with a different cross-sectional area. The scale bars in (a), (b) and (d) are 50 μm, 2 μm and 1 μm respectively.

phases [10], [12]–[17]. These issues are not directly related to the present study, which is focused on the current carrying capacity of $ZrTe_3$ nanoribbons.

The CVT-grown crystals were characterized by Raman spectroscopy, X-ray diffraction (XRD), scanning electron microscopy (SEM), energy dispersive spectroscopy (EDS), and high-resolution transmission electron microscopy (HR-TEM). Figure 1 shows Raman spectra (Renishaw) of bulk $ZrTe_3$ and exfoliated $ZrTe_3$ threads under 633 nm laser excitation for the CVT-grown material and a reference commercial sample (HQ Graphene). All spectra are consistent and in agreement with the literature [18], [19]. As expected for $P2_1/m$ symmetry, $ZrTe_3$ exhibits five main peaks in the range from 120 cm^{-1} to 250 cm^{-1}.

Mechanical exfoliation onto a Si/SiO_2 substrate was used to obtain $ZrTe_3$ nanoribbons. One should note that $ZrTe_3$ occupies an intermediate position between quasi-2D and quasi-1D materials, owing to its structure and bonding characteristics [12]–[15]. For this reason, it exfoliates into ribbon-like structures with widths larger than thicknesses; thus we refer to nanoribbons of $ZrTe_3$ *vs.* nanowires of $TaSe_3$. The length of the exfoliated nanoribbons could reach hundreds of μm. While exfoliation can often yield nanoribbons with few-nm lateral dimensions, we focused on the thickness range $\leq$50 nm and the width range $\leq$500 nm, in order to simplify device fabrication and to ensure the quality of the metal contacts.

III. Device Fabrication

We utilized the shadow mask method to directly deposit transmission line measurement (TLM) structures onto pre-selected $ZrTe_3$ nanoribbons. The exfoliated $ZrTe_3$ nanoribbons were relatively stable in the air (e.g. compared to $TaSe_3$), which allowed us to use the shadow mask method. This method was used because it avoids the damage and chemical contamination typically associated with conventional lithographic lift-off processes. It also drastically reduces the total air exposure time. The shadow masks were fabricated using double-side polished Si wafers with 3 μm thermally grown SiO_2 (Ultrasil Corp.; 500-μm thickness; P-type; <100>). The shadow mask fabrication process began with evaporation of 200 nm chromium (Cr) on the front side of the wafer (200-nm thickness), followed by a combination of electron beam lithography (EBL) and Cr etchant (1020A) to create a stencil of the TLM pattern. This was followed by fluorine-based reactive ion etching (RIE) to transfer the pattern to the underlying SiO_2. Finally, the pattern was transferred into the underlying Si substrate using the deep reactive ion etching (DRIE) (Oxford Cobra). The DRIE etch step was timed to break through to a large backside window that was previously defined using lithographic patterning, RIE, and DRIE. The shadow masks were used to fabricate $ZrTe_3$ devices by aligning them with pre-selected nanoribbons on the device substrate, clamping the aligned mask and device substrate together, and placing the clamped assembly in an electron beam evaporator (EBE) for contact deposition (10 nm Ti and 100 nm Au) through the shadow mask openings. The completed devices were then transferred to another vacuum chamber for electrical characterization. The thickness and width of $ZeTe_3$ nanoribbon were determined from the atomic force microscopy (AFM) inspection. Figure 2 shows scanning electron microscopy (SEM) images of representative Si shadow masks, as well as AFM and SEM images of the $ZrTe_3$ nanoribbon devices fabricated with the masks.

IV. Experimental Results and Discussion

The current-voltage (I–V) characteristics were measured using a probe station (Lakeshore) and a semiconductor

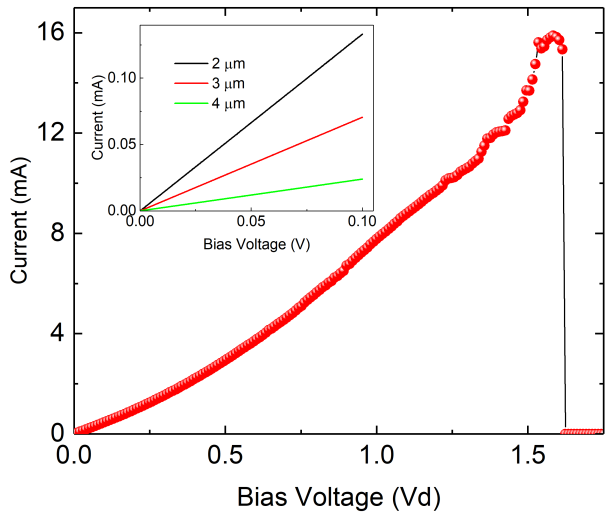

Fig. 3. High field I-V characteristics of the best quasi-1D $ZrTe_3$ nanoribbon device. The apparent breakdown current density, calculated with the AFM measured thickness and SEM measured width, corresponds to $\sim 10^8$ A/cm^2, reached at the voltage bias of $\sim$1.6 V (with a nanoribbon cross-section of $\sim$27 nm $\times$ 450 nm). The current shows some signs of instability at V $\approx$ 1.2 V indicating that some atomic threads started to break. The inset shows low-field I-V characteristics of quasi-1D $ZrTe_3$ devices with different channel lengths used for the contact resistance extraction. The data indicate the Ohmic nature of the contacts and channel.

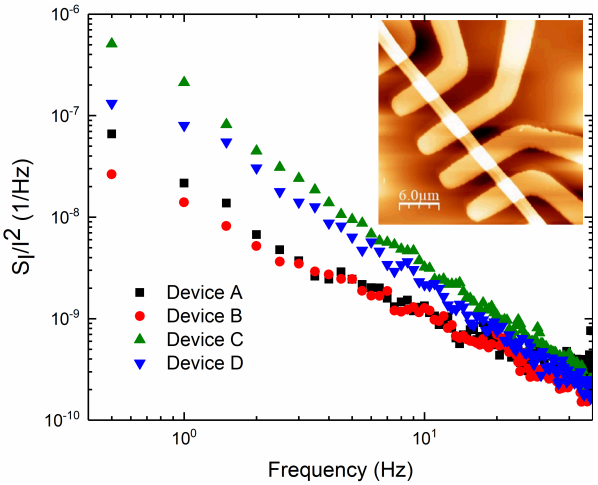

Fig. 4. Normalized noise spectrum density as a function of frequency for $ZrTe_3$ nanoribbon devices with a cross-section ranging from $\sim$27 nm $\times$ 450 nm to $\sim$100 nm $\times$ 2000 nm. The inset shows AFM image of one of the fabricated device structures.

analyzer (Agilent B1500). The low-field I-V characteristics of the devices were linear, indicating the Ohmic nature of the contacts and $ZrTe_3$ channels (see inset to Figure 3). The extracted contact resistance for typical devices was $2R_C \approx 18\Omega$, *i.e.* less than 3% of the total $ZrTe_3$ channel resistance. In Figure 3, we present I-V characteristics of a representative quasi-1D $ZrTe_3$ nanoribbon device, which was biased up to its complete breakdown. In these devices, the peak of the stressing DC current reached $\sim$15.8 mA at the bias voltage of $\sim$1.6 V. This corresponds to a maximum breakdown current density on the order of 100 MA/cm^2. Four other tested devices revealed similar current densities. The electrical resistivity did not show a clear scaling trend, fluctuating in the range from $\sim 3 \times 10^{-4}\Omega$-cm to $\sim 7 \times 10^{-4}\Omega$-cm. The obtained values are in line with the data reported in literature for bulk crystals [14], [15]. One should note that there have been reports suggesting that $ZrTe_3$ can crystalize in two polymorphs, which have either metallic or semiconducting behavior [16]. However, conditions for phase pure growth have not yet been established, in part because the structural differences between the proposed polymorphs are subtle, making the polymorphs difficult to distinguish by typical characterization techniques (*e.g.*, powder XRD). It is likely that CVT conditions yield a mixture of polymorphs, and thus one can expect a variation in resistivity depending on the dominant phase of the atomic threads.

The breakdown current density obtained for $ZrTe_3$ is a factor $\times 10$ larger than the current density at the maximum stressing current measured for Cu wires, tested before Cu introduction in the interconnect technology [20]. It is also a factor of $\times 3$ larger than the current density at the maximum stressing current for the best $TaSe_3$ nanowire devices reported to date [7]. Overall, the current density achieved in $ZrTe_3$ nanoribbons is extremely high. This can be attributed to the specific single crystalline structure of quasi-1D van der Waals materials, which minimizes electron scattering at grain boundaries and by interface dangling bonds. Measurements of the low-frequency noise (LFN) are often used to assess the material quality and reliability in conventional devices [21], [22] as well as in 2D materials and devices [23]–[25]. Figure 4 shows the noise characteristics of quasi-1D $ZrTe_3$ nanoribbons measured at room temperature. LFN is of $1/f$ type (f is the frequency). The noise spectral density $S_I/I^2 \approx 10^{-8} - 10^{-7}\text{Hz}^{-1}$ at $f = 1$ Hz is comparable to that in some other low-dimensional materials. It scales with resistance, R, as $\sim 10^{-11} \times R$, following the trend observed for carbon nanotubes, graphene and metallic nanowires [8]. The noise level can be expected to decrease further with improved material quality.

V. Conclusions

We investigated the current carrying capacity of nanoribbons made from $ZrTe_3$, a quasi-1D van der Waals material. The nanoribbon devices revealed an exceptionally high current density, on the order of $\sim$100 MA/cm^2, at the peak of the stressing DC current. Our results suggest that quasi-1D van der Waals materials that consist of single-crystals composed of MX_3 atomic threads have potential for applications in future downscaled electronic technologies.

References

[1] C. Auth, A. Aliyarukunju, M. Asoro, D. Bergstrom, V. Bhagwat, J. Birdsall, N. Bisnik, M. Buehler, V. Chikarmane, G. Ding, Q. Fu, H. Gomez, W. Han, D. Hanken, M. Haran, M. Hattendorf, R. Heussner, H. Hiramatsu, B. Ho, S. Jaloviar, I. Jin, S. Joshi, S. Kirby, S. Kosaraju, H. Kothari, G. Leatherman, K. Lee, J. Leib, A. Madhavan, K. Marla, H. Meyer, T. Mule, C. Parker, S. Parthasarathy, C. Pelto, L. Pipes, I. Post, M. Prince, A. Rahman, S. Rajamani, A. Saha, J. D. Santos, M. Sharma, V. Sharma, J. Shin, P. Sinha, P. Smith, M. Sprinkle, A. S. Amour, C. Staus, R. Suri, D. Towner, A. Tripathi, A. Tura, C. Ward, and A. Yeoh, "A 10 nm high performance and low-power CMOS technology featuring 3^{rd} generation FinFET transistors, self-aligned quad patterning, contact over active gate and cobalt local interconnects," in *IEDM Tech. Dig.*, Dec. 2017, pp. 29.1.1–29.1.4.

[2] A. P. Jacob, R. Xie, M. G. Sung, L. Liebmann, R. T. P. Lee, and B. Taylor, "Scaling challenges for advanced CMOS devices," *Int. J. High Speed Electron. Syst.*, vol. 26, no. 1, pp. 174000-1–174000-76, Mar. 2017, doi: 10.1142/S0129156417400018.

[3] J. Lienig, "Electromigration and its impact on physical design in future technologies," in *Proc. Int. Symp. Phys. Design*, Mar. 2013, pp. 33–40, doi: 10.1145/2451916.2451925.

[4] J. P. Gambino, T. C. Lee, F. Chen, and T. D. Sullivan, "Reliability challenges for advanced copper interconnects: Electromigration and time-dependent dielectric breakdown (TDDB)," in *Proc. 16th IEEE Int. Symp. Phys. Failure Anal. Integr. Circuits*, Jul. 2009, pp. 677–684, doi: 10.1109/IPFA.2009.5232553.

[5] Q. H. Wang, K. Kalantar-Zadeh, A. Kis, J. N. Coleman, and M. S. Strano, "Electronics and optoelectronics of two-dimensional transition metal dichalcogenides," *Nature Nanotechnol.*, vol. 7, no. 11, pp. 699–712, Nov. 2012, doi: 10.1038/NNANO.2012.193.

[6] H. Yang, S. W. Kim, M. Chhowalla, and Y. H. Lee, "Structural and quantum-state phase transitions in van der Waals layered materials," *Nature Phys.*, vol. 13, no. 10, pp. 931–937, Jul. 2017, doi: 10.1038/nphys4188.

[7] M. A. Stolyarov, G. Liu, M. A. Bloodgood, E. Aytan, C. Jiang, R. Samnakay, T. T. Salguero, D. L. Nika, S. L. Rumyantsev, M. S. Shur, K. N. Bozhilov, and A. A. Balandin, "Breakdown current density in *h*-BN-capped quasi-1D $TaSe_3$ metallic nanowires: Prospects of interconnect applications," *Nanoscale*, vol. 8, no. 34, pp. 15774–15782, Aug. 2016, doi: 10.1039/C6NR03469A.

[8] G. Liu, S. Rumyantsev, M. A. Bloodgood, T. T. Salguero, M. Shur, and A. A. Balandin, "Low-frequency electronic noise in quasi-1D $TaSe_3$ van der Waals nanowires," *Nano Lett.*, vol. 17, no. 1, pp. 377–383, Dec. 2016, doi: 10.1021/acs.nanolett.6b04334.

[9] G. Cheon, K.-A. N. Duerloo, A. D. Sendek, C. Porter, Y. Chen, and E. J. Reed, "Data mining for new two- and one-dimensional weakly bonded solids and lattice-commensurate heterostructures," *Nano Lett.*, vol. 17, no. 3, pp. 1915–1923, Feb. 2017, doi: 10.1021/acs.nanolett.6b05229.

[10] H. Furuseth and S. Fjellvag, "Re-examination of the crystal structure of $ZrTe_3$," *Acta Chem. Scandin.*, vol. 45, pp. 694–697, Jan. 1991, doi: 10.3891/acta.chem.scand.45-0694.

[11] J. Renteria, R. Samnakay, C. Jiang, T. R. Pope, P. Goli, Z. Yan, D. Wickramaratne, T. T. Salguero, A. G. Khitun, R. K. Lake, and A. A. Balandin, "All-metallic electrically gated 2H-$TaSe_2$ thin-film switches and logic circuits," *J. Appl. Phys.*, vol. 115, no. 3, pp. 034305-1–034305-6, Jan. 2014, doi: 10.1063/1.4862336.

[12] K. Stöwe and F. R. Wagner, "Crystal structure and calculated electronic band structure of $ZrTe_3$," *J. Solid State Chem.*, vol. 138, no. 1, pp. 160–168, Jun. 1998, doi: 10.1006/jssc.1998.7769.

[13] C. Felser, E. W. Finckh, H. Kleinke, F. Rocker, and W. Tremel, "Electronic properties of $ZrTe_3$," *J. Mater. Chem.*, vol. 8, pp. 1787–1798, Aug. 1998, doi: 10.1039/A802948B.

[14] D. J. Eaglesham, J. W. Steeds, and J. A. Wilson, "Electron microscope study of superlattices in $ZrTe_3$," *J. Phys. C, Solid State Phys.*, vol. 17, no. 27, pp. L697–L699, Sep. 1984, doi: 10.1088/0022-3719/17/27/001.

[15] S. Takahashi, T. Sambongi, J. W. Brill, and W. Roark, "Transport and elastic anomalies in $ZrTe_3$," *Solid State Commun.*, vol. 49, no. 11, pp. 1031–1034, Mar. 1984, doi: 10.1016/0038-1098(84)90416-2.

[16] R. Seshadri, E. Suard, C. Felser, E. W. Finckh, A. Maignan, and W. Tremel, "The 63 K phase transition of $ZrTe_3$: A neutron diffraction study," *J. Mater. Chem.*, vol. 8, no. 12, pp. 2869–2874, 1998, doi: 10.1039/A805427D.

[17] E. Canadell, Y. Mathey, and M. H. Whangbo, "Band electronic structure study of the semimetallic properties and the anisotropic resistivity hump in zirconium tritelluride," *J. Amer. Chem. Soc.*, vol. 110, no. 1, pp. 104–108, Jan. 1988, doi: 10.1021/ja00209a016.

[18] X. Zhu, W. Ning, L. Li, L. Ling, R. Zhang, J. Zhang, K. Wang, Y. Liu, L. Pi, Y. Ma, H. Du, M. Tian, Y. Sun, C. Petrovic, and Y. Zhang, "Superconductivity and charge density wave in $ZrTe_{3-x}Se_x$," *Sci. Rep.*, vol. 6, Jun. 2016, Art. no. 26974, doi: 10.1038/srep26974.

[19] A. Zwick, M. A. Renucci, and A. Kjekshus, "Raman scattering in the IVB transition-metal trichalcogenides: ZrS_3, $ZrSe_3$, $ZrTe_3$ and $HfSe_3$," *J. Phys. C, Solid State Phys.*, vol. 13, no. 30, pp. 5603–5614, Oct. 1980, doi: 10.1088/0022-3719/13/30/023.

[20] J. Tao, N. W. Cheung, and C. Hu, "Electromigration characteristics of copper interconnects," *IEEE Electron Device Lett.*, vol. 14, no. 5, pp. 249–251, May 1993, doi: 10.1109/55.215183.

[21] A. A. Balandin, *Noise and Fluctuations Control in Electronic Devices*. Los Angeles, CA, USA: American Scientific Publishers, Aug. 2002, pp. 27–28.

[22] L. K. J. Vandamme, "Noise as a diagnostic tool for quality and reliability of electronic devices," *IEEE Trans. Electron Devices*, vol. 41, no. 11, pp. 2176–2187, Nov. 1994, doi: 10.1109/16.333839.

[23] A. A. Balandin, "Low-frequency $1/f$ noise in graphene devices," *Nat Nano*, vol. 8, no. 8, pp. 549–555, Aug. 2013.

[24] J. Renteria, R. Samnakay, S. L. Rumyantsev, C. Jiang, P. Goli, M. S. Shur, and A. A. Balandin, "Low-frequency $1/f$ noise in MoS_2 transistors: Relative contributions of the channel and contacts," *Appl. Phys. Lett.*, vol. 104, no. 15, p. 153104, Apr. 2014.

[25] S. L. Rumyantsev, C. Jiang, R. Samnakay, M. S. Shur, and A. A. Balandin, "$1/f$ noise characteristics of MoS_2 thin-film transistors: Comparison of single and multilayer structures," *IEEE Electron Device Lett.*, vol. 36, no. 5, pp. 517–519, May 2015.